Polymer Infused Composite Metal Foam as a Potential Aircraft Leading Edge Material

Jacob C. Marx[a], *Samuel J. Robbins*[b], *Zane A. Grady*[b], *Frank L. Palmieri*[b], *Christopher J. Wohl*[b], *Afsaneh Rabiei*[a*]

[a] *Advanced Materials Research Lab, Department of Mechanical and Aerospace Engineering, North Carolina State University, Raleigh, NC, 27606, USA*
[b]*NASA Langley Research Center, Hampton, VA, 23681, USA*

*Corresponding author: Professor Afsaneh Rabiei

E-mail: arabiei@ncsu.edu

Abstract

The leading edge of the aircraft wings must be free from three-dimensional disturbances caused by insect adhesion, ice accretion, and particle wear in order to improve flight performance, safety, and fuel efficiency of the aircraft. An innovative solution was explored in this work by infusing stainless steel composite metal foam (SS CMF) with a hydrophobic epoxy resin system. S-S CMF was made with 100% stainless steel using a powder metallurgy technique. The infused epoxy filled the macro- and microporosities, unique to SS CMF's structure, creating a product with a density similar to that of aluminum. The contact angle, wear rate, erosion resistance, and insect adhesion of the novel infused composite metal foam were measured and compared to aluminum, epoxy and stainless steel. The infusion process was determined to fill up to 88% of the pores within the SS CMF and was found to reduce wettability and insect residue accretion. The contact angle of the infused SS CMF was 43% higher than its parent material, stainless steel, and 130% higher than aluminum. Insect residue maximum height and areal coverage were reduced by 60 and 30%, respectively, compared to aluminum. Grit blast experiments to simulate erosion resulted in a greater roughness increase for aluminum than for the parent epoxy resin or the resin-infused SS CMF. These results suggest that the durability and performance of infused SS CMF was superior compared to aluminum, which is the current leading edge material of choice. Based on the promising results under relevant wear and erosion conditions, it is concluded that the infused SS CMF can offer a potential tailored replacement to aluminum leading edge material.

Keywords: composite metal foam, insect residue adhesion, wear rate, erosion resistance, epoxy infusion

1. Introduction

Rain, ice, and particulate impacts erode the metallic leading edges of aircraft requiring rework and/or replacement every 5 to 10 years [1]. Future commercial aircraft designs will utilize laminar flow to a greater extent than vehicles in operation today. Topographical modifications of the wing leading edges as a result of environmental contaminants, i.e., residue buildup from insect impacts, can cause unstable airflow across the surface of the leading edge reducing the extent of laminar flow and aerodynamic efficiency of the airframe [2]. Laminar flow can be retained by implementing materials and coatings that provide anti-icing [3,4] and self-cleaning [5,6] properties. In addition, aircraft wing leading edges accumulate ice, along with other debris, that can degrade flight performance, compromise safety, and require onboard de-icing devices, which add to vehicle complexity and reduce fuel economy. A material with the durability of metals and the anti-icing/insect residues mitigation properties of functionalized polymers has a high potential to improve aircraft efficiency and safety while reducing manufacturing and operation costs. These issues are often resolved on general aviation aircraft and wind turbines through application of polymer coatings and surface treatments [7]. However, these materials do not exhibit sufficient durability for use on commercial aircraft [8].

Generally, insect fouling is a primary concern during taxi, take-off, approach, and landing where the insect population is at its highest within an altitude up to 150 meters off the ground [9,10,11]. For this reason, sacrificial films that don't erode but remove themselves under cruising flight conditions, among other approaches, have been studied for commercial use [2,12,13,]. These sacrificial coatings were removed through multiple avenues including temperature, UV exposure, and humidity. Yet, these films require constant reapplication between flights and do not provide protection during approach and landing, after the film has removed itself. Moreover, these passive

coatings also lack durability against sand and rain abrasion during flight. The work described here seeks to address these issues by infusing a hydrophobic polymer into the porosities of composite metal foam to improve the wear rate while retaining the preferable mechanical properties of the metal and hydrophobic properties of a polymer.

Metal foams represent a class of material with a relatively low density and high-energy absorption capabilities under compression [14]. They are made by creating intentional porosities within a bulk metal and are known for their unique yielding under compression, where the material strains at a constant plateau stress. Metal foams are categorized into two classes of open- and closed-cell foams, depending on the transparency and permeability of the foam. Open-cell metal foams are made of interconnected solid struts that allow liquid and gas media to easily pass through the porosities. Open-cell metal foams have previously been tested for their use in radiation shielding by filling the voids with various media such as water, borated solutions, polyethylene and wax [15,16]. On the other hand, closed-cell metal foams have porosities sealed off from their neighboring cells/pores. Closed-cell metal foams generally have little to no transparency or permeability and do not allow liquids or gases to pass through the porosities. Closed cell metal foams have found use in structural applications and energy absorption such as resistance to blast loading [17].

In this study, the porous material chosen as the base for infusion was a stainless steel composite metal foam (SS CMF), a type of metal foam defined by its extraordinary energy absorption capabilities, and mechanical properties [18,19]. The porous network within the SS CMF was infiltrated in this work with a 2-part aromatic epoxy mixed with a surface modifying agent, an aminopropyl-terminated siloxane known to improve the surface properties of epoxy coupons [20,21]. The epoxy filled the voids within and on the surface of the SS CMF generating a material

with improved wettability, reduced wear, and improved damage resistance to foreign debris for potential use as an aircraft leading edge material. The microstructure and fill efficiency of the infused SS CMF were analyzed prior to testing. In order to characterize the infused SS CMF, the wear rate, contact angle, and erosion rate were compared to that of bulk aerospace standard aluminum (6061-T6) and stainless steel (304). Insect accretion data was collected and compared for all samples following characterization. Additionally, tests were repeated on samples exposed to grit-blasting, simulating in-flight wear and degradation, to investigate the effects of wear on the material performance.

2. Materials and Processing

2.1. Composite Metal Foam

Composite metal foam (CMF) can be made of various similar and dissimilar components; this paper will focus on the infusion and testing of CMF material that are made of stainless steel (SS CMF). SS CMF is made with stainless steel hollow spheres surrounded by a stainless steel matrix. SS CMF has a comparable density to the current aerospace standard aluminum (e.g., Al 2024 T3) with almost two orders of magnitude higher energy absorption in compression and the potential to offer improved resistance to wear and debris impact [18,19]. CMF has found use in many fields of engineering structures such as fire doors and tank cars to carry hazardous materials due to its high heat dissipation [22], nuclear structures due to its radiation shielding [23], ballistic armors due to its energy absorption [24], and many crash mitigation systems for transportation due to its high energy absorption capability [25]. CMF is approximately 65-70% less dense than its parent material due to the presence of porosities within the material, making it useful for lightweight structural applications in the aviation, automotive, and armor industries. The hollow

spheres within CMF are filled with air improving the material's density, its resistance to impact at high strain rates, and enhances its ability to insulate against heat and other physical threats when compared to its parent material [22,25]. The air inside these porosities can be replaced with other materials to further modify the performance of SS CMFs in different environments [15,16].

SS CMF are normally manufactured using powder metallurgy technique. As such, the material inherently contains properties of both open and closed-cell metal foams, a unique property of SS CMF that cannot be matched with other types of metal foams. This combination of porosities enables the infusion processes to occur and can lead to a low material density relative to a bulk metal equivalent. While the cavities within the spheres perform like a closed-cell foam, the porosities created by the powder metallurgy processing of the matrix act similarly to an open-cell foam.

SS CMF was processed using a powder metallurgy technique, which has been developed and optimized in previous works [26,27]. The process starts by shaking hollow stainless steel spheres, manufactured by Hollomet GmbH (Dresden, Germany), in a stainless steel mold. The hollow spheres have a diameter of 2 mm and a wall thickness of 100 μm. Following shaking, the steel spheres create a random-loose packed arrangement with an approximate fill fraction of 59% [28]. The interstitial spaces between spheres for SS CMF were filled with a 316L stainless steel powder manufactured by North American Höganäs with a -325 mesh. The SS CMF samples were manufactured as flat panels with 100 x 50 x 15 mm dimensions and cylinders of 25 and 50 mm diameters with 100 mm length. The samples have an overall density of 2.8 g/cm^3. Figure 1 shows digital images of both sample geometries of SS CMF used in testing. SS CMF samples were cut using a Buehler Isomet 4000 saw with a diamond wafering blade into smaller samples on all sides, exposing open spheres on every surface to aid in the infusion process.

2.2. Epoxy

The resin used to infuse the SS CMF samples was an epoxy-based formulation shown to have enhanced surface properties [29]. The resin was made by mixing Ethacure 100 [Albemarle, amine hydrogen equivalent weight (AHEW) of 44.6 g/mol] diamine hardener and D.E.R.^{TM} 331 [Dow Chemical, epoxy equivalent weight (EEW) of 187.5 g/mol] resin of low molecular weight. DMS-A32 (35,800 g/mol) siloxane was added into the epoxy formulation. To achieve adhesion-reducing properties through the bulk of the resin [20], the siloxane content was maintained at 15 wt% for all experiments.

Neat epoxy control samples were prepared for comparison with the infused SS CMF samples. To cure the resin, a two-stage cure cycle was performed, according to Dow Chemical's instruction consisting of a 2 hour hold at 100 ºC followed by a 4 hour hold at 177 ºC [29].

2.3. Infusion Processing

The SS CMF samples were generated using a thermally assisted vacuum infusion technique. In this process, the SS CMF sample was placed into a thermally stable glass beaker large enough for the sample to fit without touching the sidewalls. Prior to the addition of the SS CMF sample, the beaker was coated in a silicone vacuum grease to assist in the removal of the cured product. The resin system was mixed using a Thinky (ARE 310) mixing system with 60 second mix time and 90 second degas time and poured over the SS CMF in the beaker to completely submerge the SS CMF sample. The beaker was then placed in a vacuum oven preheated to 70 ºC to reduce the viscosity of the resin and increase its fill efficiency. The absolute pressure reached 270 Pa within the oven and was held for approximately 2.5 hours. During this time, the air within the SS CMF sample escaped through the macro and micro-porosities. The infusion process was considered

complete once the air released at the surface of the resin slowed and bubbles appeared at a rate no greater than one bubble/second. The oven was then vented causing the resin to be pulled into the air evacuated porosities of the SS CMF, filling the voids within the material. Figure 2 shows a diagram of the steps taken to infuse the SS CMF. A final cure cycle of 2 hours at 100 ºC and 4 hours at 177 ºC at ambient pressure completed the infusion process. The products were then removed from the beaker and the infused SS CMF sample was cut away from the bulk epoxy that surrounded it using an electrical discharge machine (EDM).

3. Post-Infusion Experimental Procedures

3.1. SEM and Optical Imaging

The surfaces used for imaging and characterization were polished with a manual grinding station (Buehler Ecomet 3) at 100 rpm wheel rotation speed and progression from 400 to 1200 grit silicon carbide sand paper. A mirror finish was achieved by polishing the surface with a 0.05 μm alumina slurry on a polishing cloth. Optical and SEM images were taken from the surface of the polished samples Using a Leika Optical Microscope and Hitachi SU3500 SEM, respectively. The collected images were then processed and analyzed in ImageJ software [30]. Using threshold manipulation, the analysis software sharpened the images and highlighted the defining features of the metal, epoxy, and any remaining voids. The number of pixels assigned to a material's threshold range determined the approximate areal percentage of each image feature. An approximation of the infusion efficiency was calculated by taking the ratio of the final void percentage to the initial void percentage.

3.2. Wear Rate

Ascertaining the durability of a surface relative to commercial wing leading edge applications can be challenging. The variety of environmental contaminants (particulates, ice, insects, etc.) as

well as variation in the impact frequency and velocity all contribute to the complexity associated with characterizing durability. Therefore, a variety of experimental techniques were utilized to evaluate the durability of the epoxy infused SS CMF investigated in this work.

3.2.1. Pin on Disk

Wear rate analysis was conducted on flat specimens with nominal dimensions of 50.8 mm by 50.8 mm. Surface roughness measurements were conducted using a Dektak XT (Bruker) with a 12.5 μm radius tip, 3 mg of contact force, and at a resolution of 28 nm/point. At least five measurements were collected for each surface. Following grinding and polishing, the average surface roughness value (R_a) was determined to be of 0.22±0.11 μm. "Pin on Disk" (PoD) tribometry was performed on a Nanovea T50 according to ASTM G99 and utilized to evaluate surface durability. PoD tribometry uses a steel ball bearing (6 mm diameter) that runs across the surface in a small radius. The ball bearing applies an initial pressure of 30 N on the sample to initiate surface removal through frictional forces. The samples were run for a total of 500 revolutions at a rotational speed of one revolution per second. An optical profilometer (Microprof 100, FRT of America) was used to measure the gouge depth on the samples and determine the effective wear rate for each material. The optical profilometer was used to map the surface of the samples at multiple intervals of 50, 100, and 200 revolutions. Obtaining tribometric analysis representative of the wear experienced by a leading edge during operation is difficult in a lab setting. However, the PoD method gives a good approximation for comparing the wear rate and coefficient of friction of materials under consistent conditions.

3.2.2. Taber Abrasion

In addition to using the PoD method as a measurement of wear, Taber Abrasion (TA) tests were also completed to track the evolution of wear along the surface of the samples following

intervals of specified revolutions. Taber abrasion was conducted according to ASTM D4060 utilizing an H-18 (Taber Industries Calibrade Series) ceramic wheel atop the polished cylinder samples (R_a = 0.18±0.06 μm) 36.5 mm in diameter and 13 mm in height. In this case, the sample rotates below the ceramic wheel, creating a large circular wear path. The speed of rotation for the TA tests was conducted at one revolution per second. Sample roughness changes as a result of abrasion was characterized using the contact profilometer described previously. The optical profilometer was utilized to measure gouge depth and surface topology on the tested sample. The results provided insight into the wear mechanics of the infused SS CMF surface.

3.3. Contact Angle

Contact angle (CA) goniometry was used to measure the wetting properties of infused SS CMF surfaces compared to bulk aluminum, stainless steel, and the neat epoxy coupon with a similar surface finish (R_a) of < 0.6 μm (Figure 3). Interfacial tension measurements were performed to verify the purity of the water and dispersion syringe prior to conducting the contact angle measurements. Tilting axis measurements were performed in triplicate using an 8 μL water droplet. Interfacial tension values and advancing water contact angle values were determined using line-fitting algorithms provided by First Ten Angstroms. The measurements were completed using a FTA1000B contact angle goniometer (First Ten Angstroms). A contact angle goniometer interrogates the interface between a surface and a liquid droplet and provides the angle on either side of the droplet. The infusion process described herein aims to increase the hydrophobic properties of SS CMF as indicated by an increase in contact angle value compared to the conventional metals such as steel and aluminum. The measurements were conducted on flat samples with 20 x 40 x 8 mm dimensions. The samples were polished to a R_a of 0.22 μm. The contact angle measurements generated from the initial samples are referred to “as polished” data.

CA measurements were also conducted on Taber Abrasion samples following 150, 300, 450, and 600 revolutions. The contact angle measurements were conducted along the ceramic wheel's rolling path at a 0º tilt and described the evolution of wettability of the surface under controlled wear.

The contact angle measurements were also repeated on samples eroded using the erosion protocol described in Section 3.4. The resulting data is referred to as the long-term erosion (LTE) contact angle data, and is collected as a representation of in-flight wear.

3.4. Surface Erosion Rate and Simulated Long Term Erosion

The erosion rate was calculated by measuring the material loss at a specific point of the surface following 120 seconds of localized sandblasting of a micro-grit abrasive media on 50.8 by 76.2 mm flat specimens with initial surface roughness similar to what was described for previous durability measurements at a constant nozzle pressure of 0.69 MPa. The blast media (180 grit alumina) was isolated to a small area by covering the rest of the sample with a thin stainless steel mask that contained a hole with an approximate area of 2 mm^2. The nozzle was held approximately 25.4 mm from the surface. The micro-grit impact removed material from the sample surface creating deformities within a small area on the surface. The deformities' depths were measured using the optical profilometer and the associated erosion rate was calculated for each sample as a metric for wear in addition to the tribology tests performed through PoD and Taber Abrasion. Additional microgrit blasting experiments were conducted over a larger surface area to observe the change in surface roughness arising from material removal. This approach was used to mimic surface roughening during LTE that occurs along the leading edges due to impact from rain, ice, and micro-debris. Other researcher have utilized similar approaches to evaluate the influence that particulate erosion has on an aircraft surface [31-34]. A box coat method was implemented, in

which the samples were sprayed at a constant distance from the nozzle for 120 seconds for each testing surface. The resulting change in surface roughness values was compared to aluminum and neat epoxy coupons exposed to the same conditions.

3.5. Insect Residue Adhesion

Insect residue adhesion tests have been used to measure the insect buildup vertically and radially for leading edge materials [35-39]. In this study, insect residue adhesion tests were completed using a pneumatic insect delivery device on the flat samples polished to a similar surface finish of 0.22 μm with 100 x 50 x 15 mm in size. The pneumatic insect delivery device consists of a Venturi vacuum pump positioned within a benchtop wind tunnel [35]. When pressurized air passes through the vacuum pump, a suction force is generated and is utilized to draw an insect into the airstream. The wind tunnel provides airflow rates of approximately 9 m/s and minimizes air stagnation around the test surface. Flightless fruit flies (*Drosophila melanogaster*) of the order Diptera were selected to impact the samples due to their ease to handle in the wind tunnel and their relatively high population across the United States. The order Diptera refers to insects with one pair of wings and are generally used in insect impact tests due to their relatively smaller size (1-3 mm) and more abundance during take-off and landing [38]. Each sample was impacted three times, with care taken to avoid overlap of residues from neighboring impact zones. The surfaces of the samples were scanned following impact tests using an optical profilometer (FRT of America, Microprof 100 at a resolution of 5 μm between data points) to determine the areal coverage of insect residues as well as the maximum insect residue height. An ideal material would have limited insect residue accretion upon insect impact, which would lead to better retention of laminar flow over an aircraft wing leading edge resulting in improved fuel efficiency. The insect impact adhesion tests were conducted on as-polished and samples eroded

using micro-grit sandblasting along the testing surface (discussed in Section 3.4), imitating in-flight abrasion and wear.

Table 1 summarizes the extensive number of tests and analyses completed on these materials, as well as their dimensions and initial surface roughness values.

4. Results and Discussion

4.1. SS CMF manufacturing and microstructure

Inherent matrix voids in SS CMF can be seen between the particles following sintering (Figure 4). Some of the voids remained open after sintering and created micro-channels used for infusing SS CMF, as can be seen in the SEM image of the final sintered product in Figure 4.

The hollow spheres were also processed using powder metallurgy technique. For this reason, micro-porosities exist within the sphere walls, allowing for further penetration of resin into the SS CMF. The sphere walls were designed to contain an approximate wall porosity of 5%. Figure 4(c)-(d) show SEM images highlighting the micro-porosities within the sphere walls, that facilitate the infiltration of gases and liquids through the entire thickness of SS CMF. These porosities create a tortuous path to the hollow metal spheres cavity allowing the epoxy and any other liquids to seep through the matrix and fill the hollow spheres. For this reason, composite metal foam processed using powder metallurgy technique has unique characteristics of both closed-cell and open-cell metal foam that lend to infusing it through the entire thickness while maintaining retention of the resin.

The percentage of porosities within the SS CMF material was calculated to be 65%. This value is calculated by dividing the measured density of the SS CMF sample by the density of the parent material, or in this case bulk 316 stainless steel, and subtracting the result from 100%.

4.2. Imaging and Infusion Efficiency

The processed optical images of the infused SS CMF surface are shown in Figure 5. Figure 5(a) is the unaltered image prior to analysis and pixel manipulation with ImageJ, while Figure 5(b)-(d) represent the infused epoxy, metal and voids make-up of the material. The threshold was set to isolate each material and calculate the approximate percentage of stainless steel, epoxy, and voids on the surface. Threshold analysis indicated that the captured micrograph consisted of approximately 40% stainless steel (matrix and sphere wall), 53% epoxy, and 7% un-infused voids. The infusion efficiency was calculated using the following equation:

$$Infusion\ Efficiency = \frac{P_i - P_f}{P_i} \times\ 100\%$$

where P_f is the final porosity left in SS CMF after infusion, and P_i is the initial porosity content prior to infusion. The initial porosity is equal to the sum of the final void percentage and the epoxy fill, or about 60%. This indicates that the infusion process was able to accomplish a fill efficiency of 88% across the surface. Ideally, the infusion efficiency for open porosities can be improved through optimized processing by either increasing the system's time under vacuum or increasing the applied vacuum.

It is worth noting that the SS CMF samples infused in this study were cut along each side, revealing a random arrangement of sphere openings on the surface. An example of such cut surface is shown in Figure 6 (optical image of the surface of an infused SS CMF sample). The red arrows point to the various sized voids on the surface that are created by cutting the spheres. This, however, is not the only surface arrangement that can be obtained through cutting SS CMF. Alternatively, SS CMF can be manufactured and cut in such a way that it can expose varying surface percentage of voids when the cut goes along an organized sphere arrangements at varying depths.

Figure 7 is a diagram of organized spheres at the bottom of a SS CMF panel. The red lines represent cuts into the material exposing varying depths of the macro-porosities. Consequently, the amount of epoxy which can be exposed at the surface can vary depending on the cutting line position. As the cuts move farther into the spheres' diameters (from cuts 1 to 3), a higher ratio of epoxy is exposed on the surface. This enables determination of an optimized ratio of exposed contact areas in order to obtain and maximize a specific surface property. Note that this will not change the infusion on the interior of the sample, but can be used to fine tune desired surface properties [27].

4.3. Wear Rate

4.3.1. Pin on Disk

The optical profilometer maps showing the evolution of wear along the PoD path at 50, 100 and 200 revolutions for the bulk aluminum, bulk stainless steel, and infused SS CMF is shown in Figure 8. As can be seen, the aluminum had the deepest gouge formation, represented by the dark valleys and brightly colored peaks created at the edge of the gouge. The infused SS CMF has the lowest tribometric wear compared to the other metal samples as seen by the lack of a wear path. The infused SS CMF did not accumulate nearly as much debris along the ball bearing's path as the other metallic samples, as can be seen by the image collected after 200 revolutions.

The wear rate of each sample was determined by measuring the gouge depth created by 500 revolutions on the tribometer. The relative wear rates and material coefficients of friction are graphed in Figure 9 and Figure 10, respectively. The wear rates are presented in relation to each other with higher wear rates above the central line and lower rates falling below. Materials with a higher wear rate are expected to have shorter lifetimes in service, as it corresponds to a deeper gouge created by the steel ball. As can be seen in Figure 9, aluminum had the highest wear rate of

all materials tested. This was likely due to the softness of aluminum compared to bulk stainless steel and SS CMF samples. The epoxy, although it is quite soft, had a much lower coefficient of friction against the steel ball. As the coefficient of friction increases across the surface of the sample, so does the shear force and subsequent accumulation of damage and debris on the surface. The infused SS CMF sample had a lower wear rate than the stainless steel, outperforming its parent metal by retaining properties of the infused epoxy. The infused SS CMF exhibited a measured coefficient of friction 30% lower than that of both the stainless steel and aluminum as can be seen in Figure 10.

4.3.2. Taber Abrasion

The Taber Abrasion tests consisted of two parts: (1) the wear analysis following cyclic revolutions and (2) repeated contact angle measurements at 150 revolution intervals. Contact angle measurement results will be presented in Section 4.4.1, following the discussion of the as-polished data. The optical profilometry images for SS CMF before and after 600 revolutions are shown in Figure 11(a) and (b), respectively, while Figure 11(c) and (d) show optical microscope images of the same locations. Comparing the optical profilometry images, it can be seen on the left edge of Figure 11(b) that large pores on the surface were susceptible to the loss of epoxy from the surface (caving in). The optical microscope images revealed the eventual roughening of the surface as epoxy was removed from the small voids in SS CMF surface Figure 11(c). However, comparing the surface roughness data between the infused SS CMF and neat epoxy surfaces revealed similar wear performance, indicating that the infused resin was well bonded to the SS CMF porosities and provided a superior abrasion resistance to the infused SS CMF samples. These comparisons of surface roughness data for various samples will be discussed in further detail in Section 4.5.

4.4. Contact Angle

4.4.1. As-Polished Results

Contact angle measurements made on the as-polished surfaces at 0º and 60º tilt are shown in Figure 12. The infused SS CMF had an initial contact angle at 0º tilt higher than the epoxy resin, stainless steel, and aluminum samples. This relationship between surfaces is retained in the advancing water contact angle values at a 60 º tilt as can be seen in Figure 3. However, the infused SS CMF exhibited a receding water contact angle value that was lower than the epoxy resin (Figure 12(b)). This indicated that the water contact line was being pinned to the hydrophobic/hydrophilic interfaces between epoxy and metal domains. The receding contact angle of the infused SS CMF remained higher than both the stainless steel and aluminum, outperforming the aerospace grade aluminum by 30% and 130% at 0º and 60º tilt, respectively. The infused sample had a receding contact angle 43% greater than its parent metal, stainless steel.

4.4.2. Contact Angle Values After Taber Abrasion

Contact angle values were measured on epoxy coupon, bulk stainless steel, bulk aluminum, and infused SS CMF surfaces at 0º tilt after being subjected to intervals of 150 revolutions Taber abrasion. The results are shown in Figure 13(a). The data shows that the infused SS CMF consistently had a higher contact angle value than both the stainless steel and aluminum samples at each interval. The epoxy coupon had the highest contact angle value measured, well above 100º following the initial measurement and 115º following 600 revolutions, as shown in Figure 13(c). The infused SS CMF continued to exhibit a wettability between that of the epoxy resin and stainless steel and a contact angle well above the bulk aluminum, which varied between 60 and 80º throughout multiple revolutions. Figure 13(b) is an image of the water droplet measured on

the infused SS CMF showing the large contact angle on its advancing side. The droplet is slightly offset due to the epoxy within a sphere collapsing below the surface after the abrasion testing.

4.5. Erosion Rate and Surface Roughness Evolution

The results of the erosion created by localized grit blasting are presented in Table 2. Consistent with the previously measured properties, the infused SS CMF had an erosion rate between that of the epoxy and stainless steel. The stainless steel sample had the lowest erosion rate, primarily due to its high hardness. Finally, the epoxy had the highest wear rate among the tested materials. The erosion rate for the infused SS CMF sample was 67% lower than that of the epoxy coupon, which was due to the presence of the hard stainless steel matrix surrounding epoxy-filled pores.

Surface roughness evolution testing was conducted on all samples in order to better understand the durability of the infused SS CMF under long term use and wear, not just localized erosion. The results shown in Figure 14 compare the trends of the average surface roughness (R_a) after 0, 120, and 240 seconds of sandblasting. Initially the infused SS CMF and aluminum showed a similar R_a of 0.23 μm. At both intervals of 120 seconds of sandblasting, it was found that the epoxy had a lower average surface roughness than both the aluminum and infused SS CMF. This occurred due to the material's ability to evenly wear across the surface when exposed. The metal samples had a larger average surface roughness with the aluminum peaking at approximately 3.25 μm. The surface roughness of the infused SS CMF was 33% lower than the aluminum after 120 seconds and 17% lower after 240 seconds of micro-grit blasting. This data showed the benefit of using infused SS CMF for its simulated long-term erosion resistance.

4.6. Insect Adhesion

The insect residue height and areal coverage of each surface after insect impact testing are presented in Figure 15 and Figure 16. Lower values for both the insect residue height and areal

coverage are preferable as larger insect residue accretions may result in premature transition from laminar to turbulent flow [2]. From the initial results, the infused SS CMF had a similar insect impact height to stainless steel and a lower measured height than aluminum (60% lower). Additionally, the measured impact area of the infused SS CMF was 30% lower than aluminum and 64% lower than stainless steel. The reduction in buildup height can be attributed to the stainless steel matrix, while the reduction in areal coverage was attributed to the infused epoxy resin. As such, the infused SS CMF reduced insect residue accretion better than the other metal surfaces. Large error bars are typical for these experiments due to differences in the fruit fly size and age and slight variation in the exact velocity at the time of impact.

5. Long-Term Erosion Results and Discussion

5.1. Wear Rate

The wear rates measured using the PoD method of the long-term erosion samples are plotted alongside the initial as-polished results in Figure 17. Note that the LTE was only completed on the infused SS CMF, stainless steel, and aluminum samples and is not presented for the neat epoxy as grit stuck within the sample surface greatly skews the recorded measurements. From Figure 17 it can be seen that the infused SS CMF outperforms both stainless steel and aluminum in as-polished and long-term eroded conditions. The wear rate of the SS CMF did not change significantly after exposure to LTE. However, the stainless steel showed an increase in wear rate with a higher surface roughness created by the sandblasting (marked by LTE). The aluminum, on the other hand, had an improved wear rate after being blasted with micro-grit media, as is shown by the reduction in wear rate for the LTE sample. The rougher surface created by the sandblasting had a higher coefficient of friction than the as-received material, as can be seen in Figure 18. Investigation of the infused

SS CMF's material properties under long-term operating conditions, mimicked by the sandblasting, yielded optimistic results for the material's wear rate and coefficient of friction.

5.2. Contact Angle

The contact angle of the metallic samples treated by sand blasting media for LTE testing are compared to that of the as-polished samples reported in Figure 19 and reveal a general reduction in contact angle on LTE samples. The reduction can be explained by Wenzel [40], as a rougher surface exposes a large surface area to interact with the droplet and magnifies its inherent wettability. As such, hydrophilic surfaces such as metals become increasingly hydrophilic, leading to a reduced contact angle. Hydrophobic materials, such as the epoxy, are likely to exhibit an increase in contact angle due to increased surface roughness. The mechanism described by Wenzel varies for the infused SS CMF sample as it contains a combination of hydrophilic and hydrophobic materials. While the roughened epoxy surface was expected to decrease the wettability with increasing surface roughness, the metallic part of the SS CMF will have a reduced contact angle by increased roughness. Moreover, any removed epoxy from the infused SS CMF exposes the metal below and its inherently high wettability reduces the contact angle at both 0º and 60º tilt. The infused SS CMF became increasingly hydrophilic upon increasing surface roughness created by sandblasting (Figure 19(a)). As such, the contact angle decreased from 95º to 89º for the as-received infused SS CMF to the infused SS CMF-LTE. The rougher surface reduced the contact angle of the infused SS CMF at 0º and 60º by 6% and 11% respectively. Whereas, the stainless steel sample exhibited a contact angle value reduction of 41% and 40% upon roughening of the surface through sandblasting for 0º and 60º tilt measurements, respectively. This was a much larger reduction in contact angle than that measured on the infused SS CMF sample. Compared to the control stainless steel sample, the presence of the epoxy appears to have mitigated the loss of

wettability across the surface of the infused SS CMF, showing a retention of the infused properties even after additional erosion. The aluminum also demonstrated contact angle degradation at 0º tilt. The infused SS CMF sample had a contact angle consistently 50% higher than aluminum, making the infused SS CMF the preferable leading edge material to maintain hydrophobicity, while noting the infused SS CMF and bulk aluminum have similar densities. At a 60º tilt the minimum contact angle of the aluminum increased from the initial measurement. This may be due to surface features pinning the water droplet which would likely and rapidly become hydrophobic due to the near instantaneous generation of an aluminum oxide layer on the freshly exposed aluminum surfaces. Although the aluminum's contact angle value increased under tilt, the infused SS CMF consistently maintained a larger contact angle and preferable hydrophobic properties.

5.3. Insect Adhesion

The LTE data for insect residue height and areal coverage are plotted alongside the as-polished results in Figure 20 and Figure 21, respectively. The LTE treatment revealed a general reduction of the insect residue height and areal coverage in most samples. Sandblasting effectively enhanced the roughness of the materials' surfaces, improving their resistance to insect residue accretion [36]. Both the stainless steel and aluminum samples' insect residue height and areal coverage were drastically reduced following sandblasting. Meanwhile, the infused SS CMF's impact height increased while the total residue areal coverage decreased. The data is slightly skewed for the insect height measurements of the LTE infused SS CMF samples as it was found that a limb had remained adhered upright along the surface, similar to what occurred with the epoxy coupon, yielding an average much higher than the other measurements taken on the same surface.

6. Conclusion

Initial results indicate that resin-infused composite metal foam materials can provide greater durability and wear resistance, lower wettability and insect residue accretion and extended operational lifetime, compared to aerospace grade aluminum or an organic coating solution for airplane's leading edge. The infusion process of the SS CMF proved to be successful, obtaining an 88% infusion efficiency. The inherent structure and porosity of the material aids in the infusion process, and improves retention of the resin system even after exposing the surface to micro-grit erosion. The measured material properties of the infused SS CMF consistently fall between that of the stainless steel and the infusing resin system that make up its surface. The hydrophobic properties of the surface was over 130% better than that of the aerospace standard aluminum. Additionally, the infused SS CMF was found to have a coefficient of friction 30% lower than both the aluminum and stainless steel, which in turn improves the lifetime and susceptibility to wear and erosion during service. Compared to standard aluminum, insect impact testing reveals the infused SS CMF has a 60% lower insect residue height and 30% lower areal coverage. Micro-grit erosion treatment was used to explore the wear and erosion resistance of the materials, similar to what is experienced during flight. Overall, the initial findings of this study show that epoxy infused SS CMF outperforms aluminum under multiple testing conditions. The infused SS CMF also retains its properties through erosion and wear, improving lifetime of the leading edge and reducing its maintenance costs and down time. Further studies on the ice adhesion on infused SS CMF compared to control aerospace grade aluminum is ongoing.

Acknowledgments

This project was funded by the NASA Langley Research Center IRAD program, project #NNX17AD67A.

References

1. C. Sriram, A. Haghani, An optimization model for aircraft maintenance scheduling and re-assignment. Transportation Research Part A: Policy and Practice. 37(1) (2003) 29-48.
2. M. Kok, J.G. Smith Jr., C.J. Wohl, E.J. Siochi, T.M.Young, Critical considerations in the mitigation of insect residue contamination on aircraft surfaces—a review, Prog. Aerosp. Sci. 75 (2015) 1-14.
3. Y.H. Yeong, A. Milionis, E. Loth, J. Sokhey, A. Lambourne, Atmospheric ice adhesion on water-repellent coatings: wetting and surface topology effects, Langmuir. 31 (2015) 13107-13116.
4. J. Lv, Y. Song, L. Jiang, J. Wang, Bio-inspired strategies for anti-icing, ACS Nano. 8 (2014) 3152-3169.
5. V.A. Ganesh, H.K. Raut, A.S. Nair, S. Ramakrishna, A review on self-cleaning coatings, J. Mater. Chem. 21 (2011) 16304-16322.
6. A. Milionis, R. Giannuzzi, I.S. Bayer, E.L. Papadopoulou, R. Ruffilli, M.Manca, A. Athanassiou, Self-cleaning organic/inorganic photo-sensors, ACS Appl. Mater. Interfaces. 5 (2013) 7139-7145.
7. S. Zhang, K. Dam-Johansen, P. L. Bernad Jr., S. Kiil, Rain erosion of wind turbine blade coatings using discrete water jets: Effects of water cushioning, substrate geometry, impact distance, and coating properties, Wear. 328 (2015) 140-148.
8. R.J. Varley, E.K. Simmonds, J.E. Seebergh, D.H. Berry, Investigation of factors impacting the in-service degradation of aerospace coatings, Progress in Organic Coatings. 74 (2012) 679-686.
9. F. Smith, D.J. Higton, Flight Tests on King Cobra FZ.440 to investigate the practical requirements for the achievement of low profile drag coefficients on a low drag aerofoil, Aeronaut. Res. Council R&M. 1945, 2375.
10. J.L. Maresh, M.B. Bragg, The Role of Airfoil Geometry in Minimizing the Effect of Insect Contamination of Laminar Flow Sections, AIAA. 84 2170 (1984).
11. C.C. Croom, B.J. Holmes, Flight Evaluation of an Insect Contamination Protection System for Laminar Flow Wings, SAE Paper 850860 (1985).
12. V. Stenzel, Y. Wilke, S. Schrubbers, A. Hartwig, G. Niedzwiedzkl, S. Grunke, Method for protecting the surface of an aircraft against contamination with insect residues and/or icing, U.S. Patent No. 2012/0160963 A1 (2012).
13. I.S. Bayer, K.G. Krishnan, R. Robison, E. Loth, D.H. Berry, T.E. Farrell, J.D. Crouch, Thermal alternating polymer nanocomposite (TAPNC) coating designed to prevent aerodynamic insect fouling. Scientific Reports (Nature Publisher Group) 6 (2016) 38459.
14. M. F. Ashby, A. G. Evans, N. A. Fleck, L. J. Gibson, J. W. Hutchinson, H.N.G. Wadley, Metal Foams: A Design Guide, Butterworth-Heinemann, 2000.
15. S. Xu, M. Bourham, A. Rabiei, A novel ultra-light structure for radiation shielding, Materials & Design. 31 (2010) 4 2140-46.
16. S. Chen, M. Bourham, A.Rabiei, Novel Light-Weight Materials for Shielding Gamma Ray, Rad. Phys. and Chem. 96 (2014) 27–37.
17. J. Marx, M. Portanova, A. Rabiei, A study on blast and fragment resistance of composite metal foams through experimental and modeling approaches, Composite Structures, (2018), doi:10.1016/j.compstruct.2018.03.075.

18. A. Rabiei, L.J. Vendra, A Comparison of Composite Metal Foam's Properties and Other Comparable Metal Foams, Materials Letters. 63 (2009) 5 533–36.
19. J. Marx, A. Rabiei, Overview of Composite Metal Foams and Their Properties and Performance, Adv. Eng. Mat. 19 (2017) 1600776.
20. C.J. Wohl, B.M. Atkins, M.A. Belcher, J.W. Connell, Synthesis, characterization, topographical modification, and surface properties of copoly(imide siloxane)s. High Perform Polymers. 24 (2012) 140–149.
21. J.W. Connell, C.J. Wohl, A.M. Crow, W.T. Kim, M.H. Shanahan, J.R. Doss, Y. Lin, Synthesis and characterization of copolyimides containing fluorine and silicon surface-modifying agents, High Performance Polymers. (2017) 1-10.
22. S. Chen, J. Marx, A. Rabiei, Experimental and Computational Studies on the Thermal Behavior and Fire Retardant Properties of Composite Metal Foams, Int. J. of Therm. Sci. 106 (2016) 70–79.
23. S. Chen, M. Bourham, A. Rabiei, Attenuation Efficiency of X-Ray and Comparison to Gamma Ray and Neutrons in Composite Metal Foams, Rad. Phys. and Chem. 117 (2015) 12–22.
24. M. Garcia-Avila, M. Portanova, A. Rabiei, Ballistic Performance of Composite Metal Foams. Comp. Struct. 125 (2015) 202–211.
25. Y. Alvandi-Tabrizi, A. Rabiei, Use of Composite Metal Foam for Improving Absorption of Collision Forces, Procedia Mat. Sci., 8th International Conference on Porous Metals and Metallic Foams, no. 4, Supplement C (January 1, 2014) 377–82.
26. B.P. Neville, A. Rabiei, Composite Metal Foams Processed through Powder Metallurgy, Mat. & Design. 29 (2008) 2 388–396.
27. A. Rabiei, L. Vendra, N. Reese, N. Young, B.P. Neville, Processing and Characterization of a New Composite Metal Foam, Mat. Trans. 47 (2006) 9 2148–2153.
28. A. Rabiei, A.T. O'Neill, A Study on Processing of a Composite Metal Foam via Casting, Mat. Sci. and Eng.: A. 404 (2005) 1-2 159–64.
29. C.J. Wohl, J.G. Smith Jr., J.M. Gardner, R.K. Penner, J.W. Connell, E.J. Siochi, In Novel Epoxy Particulate Composites for Mitigation of Insect Residue Adhesion on Future Aircraft Surfaces, 37th Annual Meeting of the Adhesion Society, San Diego, CA, February 23-26; San Diego, CA, 2014.
30. ImageJ., 2015. National Institutes of Health.
31. F. Salazar, A. Barrientos, Surface roughness measurement on a wing aircraft by speckle correlation. Sensors (2013) *13*(9), 11772-11781.
32. J.E. Goodwin, W. Sage, G.P. Tilly, Study of erosion by solid particles. Proceedings of the Institution of Mechanical Engineers (1969) *184*(1), 279-292
33. S. Dhar, T. Krajac, D. Ciampini, M. Papini, Erosion mechanisms due to impact of single angular particles. Wear (2005) *258*(1-4), 567-579.
34. F. Cernuschi, C. Guardamagna, S. Capelli, L. Lorenzoni, D.E. Mac, A. Moscatelli, Solid particle erosion of standard and advanced thermal barrier coatings. Wear (2016) *348*, 43-51.
35. C.J. Wohl, J.G. Smith, R.K. Penner, T.M. Lorenzi, C.S. Lovell, E.J. Siochi, Evaluation of Commercially Available Materials to Mitigate Insect Residue Adhesion on Wing Leading Edge Surfaces, Progress in Organic Coatings 76 (2013) 1 42–50.

36. M. Kok, D. Raps, T. Young, Effects of surface roughness and energy on insect residue adhesion to aircraft leading edge surfaces, Adhesion Society Annual Meeting, Daytona Beach, FL (2013).
37. K.G. Krishnan, A. Milionis, F. Tetteh, E. Loth, Fruit Fly Impact on an Aerodynamic Surface: Types of Outcomes and Residue Components, Aerospace Sci. and Tech. 69 (2017) 181–92.
38. J.A. Freeman, Studies in the distribution of insects by aerial currents – the insect population of the air from ground level to 300 feet, J. Anim. Ecol. 14 (1945) 128-154.
39. W.S. Coleman, Roughness due to insects. G.V. Lachmann (Ed.), Boundary Layer and Flow Control, vol. II, Pergammon Press, Oxford (1961), pp. 628-747.
40. R. N. Wenzel, Resistance if Solid Surfaces to Wetting by Water, Industrial & Eng. Chem. 28 (1936) 8 988-994.

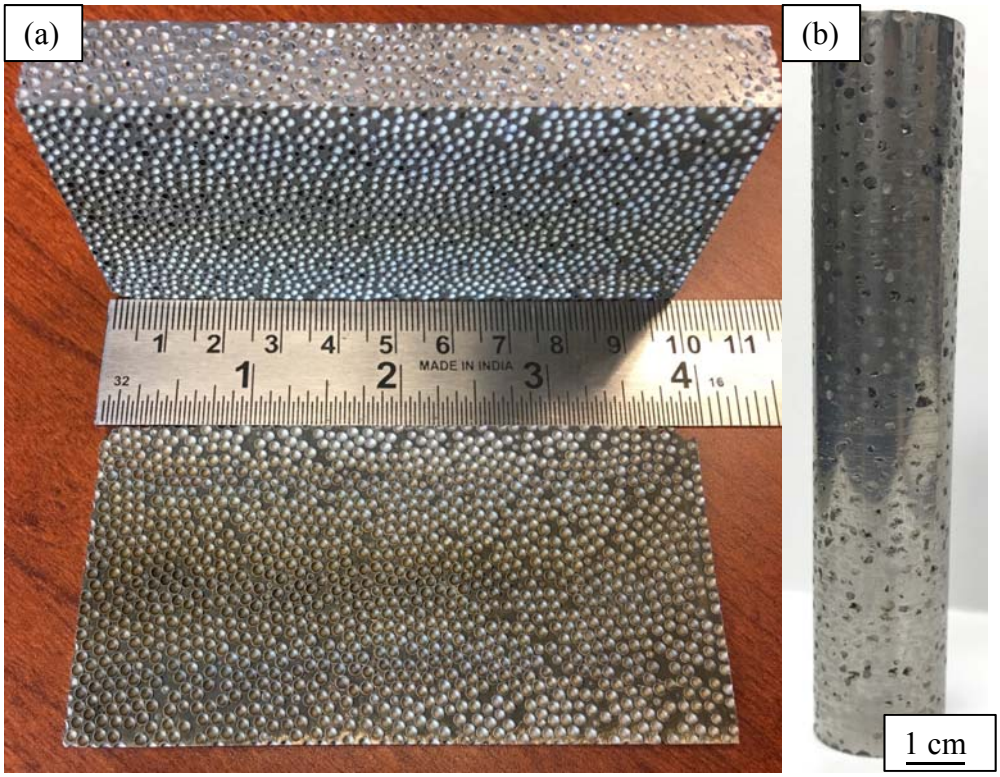

Figure 1. Images of SS CMF manufactured by powder metallurgy technique (a) a flat panel and (b) cylinder.

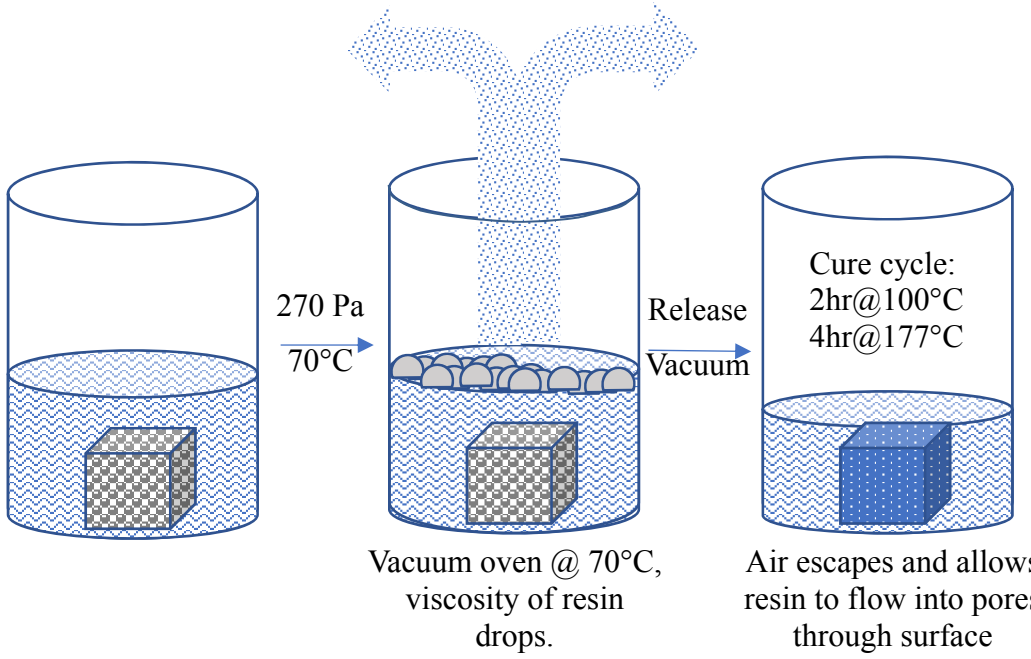

Figure 2. Diagram of the vacuum infusion process used to create the epoxy infused SS CMF.

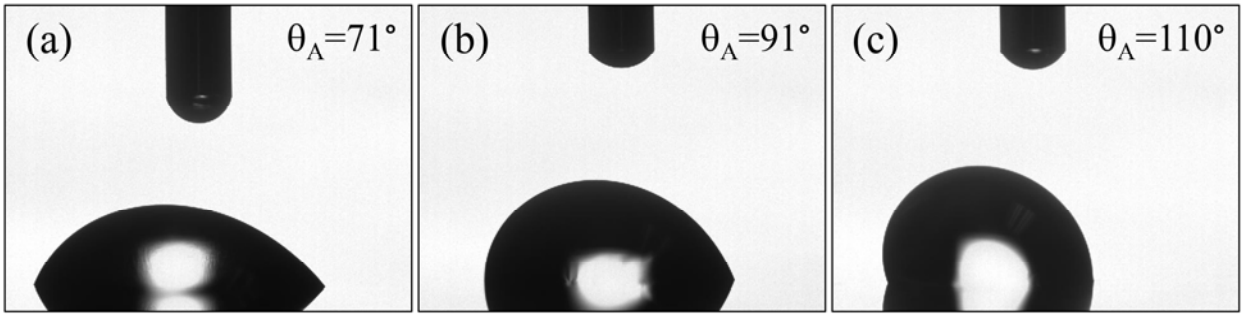

Figure 3. Tilting axis (60°) water contact angle values measured on (a) stainless steel, (b) epoxy resin A32, and (c) infused SS CMF.

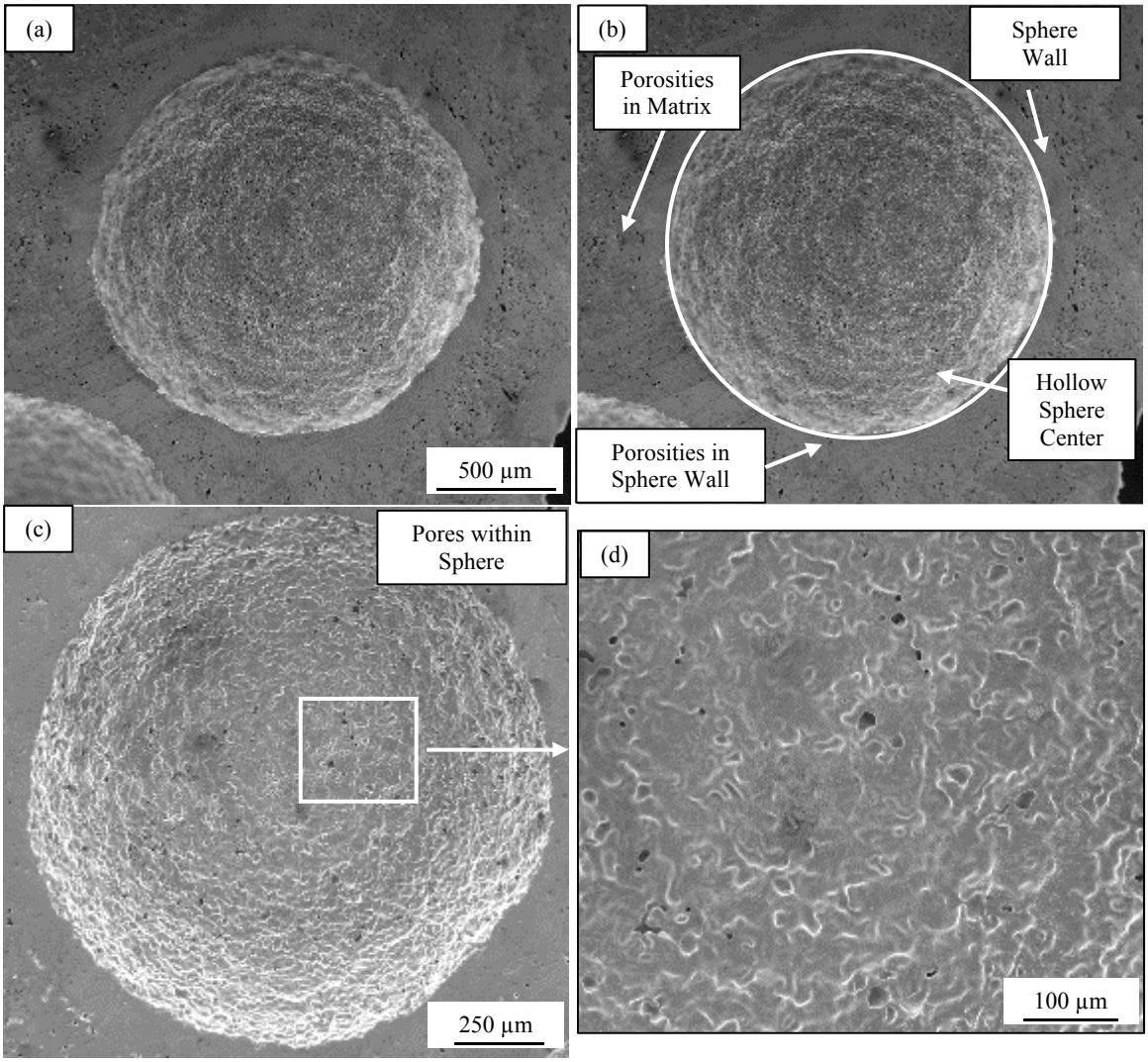

Figure 4. (a) SEM Images of the initial porosities surrounding a sphere in SS CMF with (b) the areas of interest highlighted in white. (c) SEM Images of the interior surface of a hollow sphere showing the (d) internal porosities within the sphere wall.

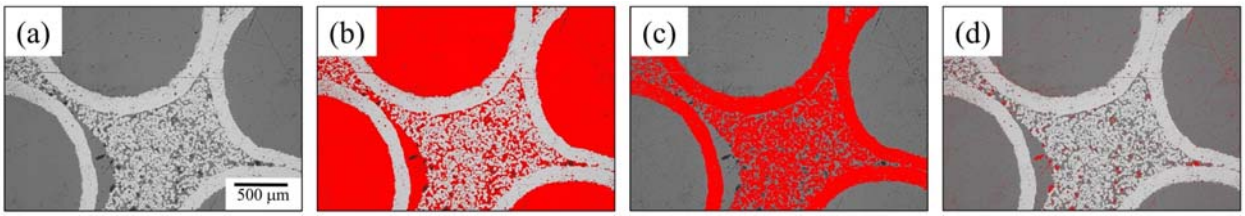

Figure 5. (a) Optical microscope image of infused SS CMF used to determine the infusion efficiency through ImageJ process highlighting the (b) infused epoxy, (c) metal and (d) voids that make up the material.

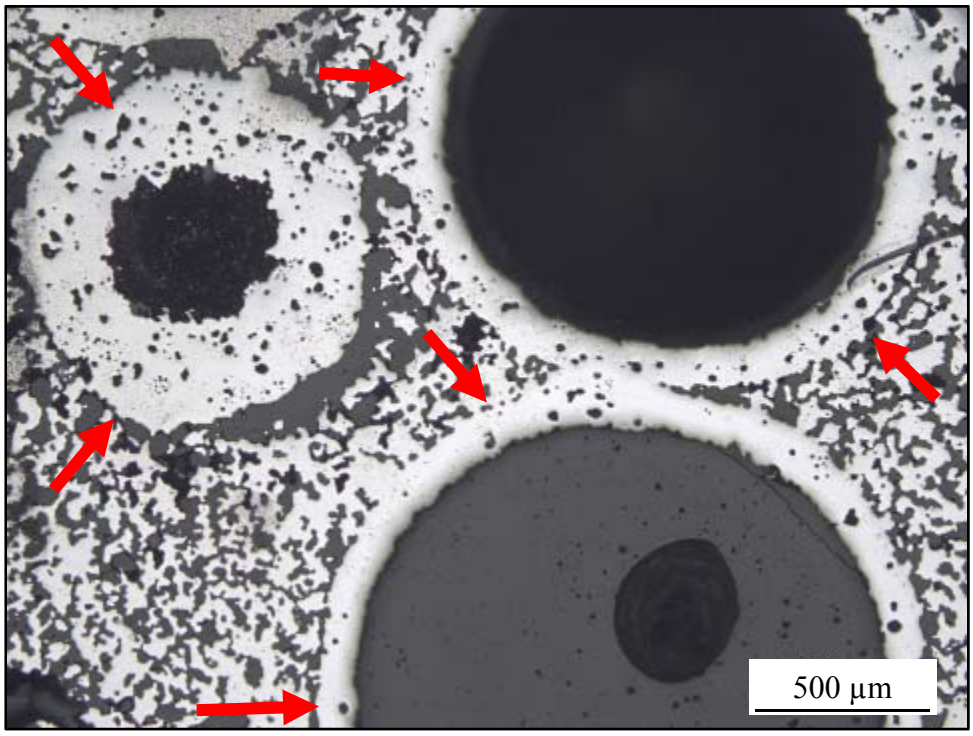

Figure 6. Optical microscope image of infused SS CMF showing sphere openings on the surface with varying sizes. Sphere walls are shown by arrows.

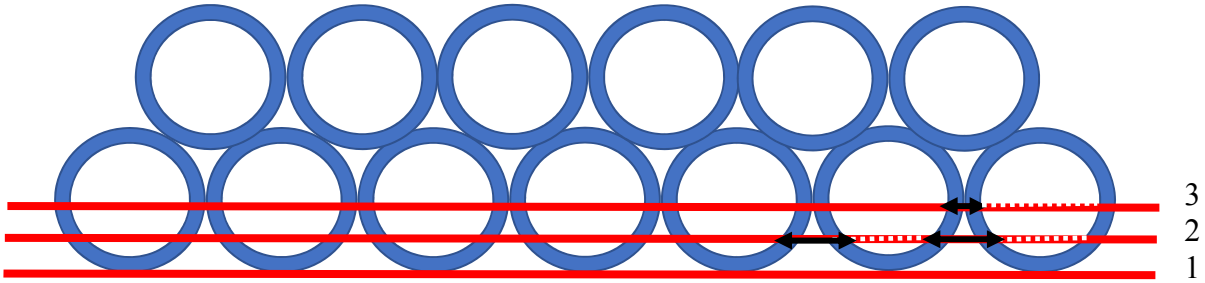

Figure 7. Hollow sphere arrangement at the bottom of a SS CMF panel highlighting various cuts that can be made to tailor surface properties of infused SS CMF in order to optimize its performance for certain applications. The cuts shown are (1) a surface cut without exposing the macro-porosities within the spheres, (2) sphere cut exposing an almost equal area of epoxy (shown with dotted line) and steel (shown with double arrow line) on the surface, and (3) a deeper cut exposing larger area of epoxy (dotted line) and less steel (double arrow line) at the surface.

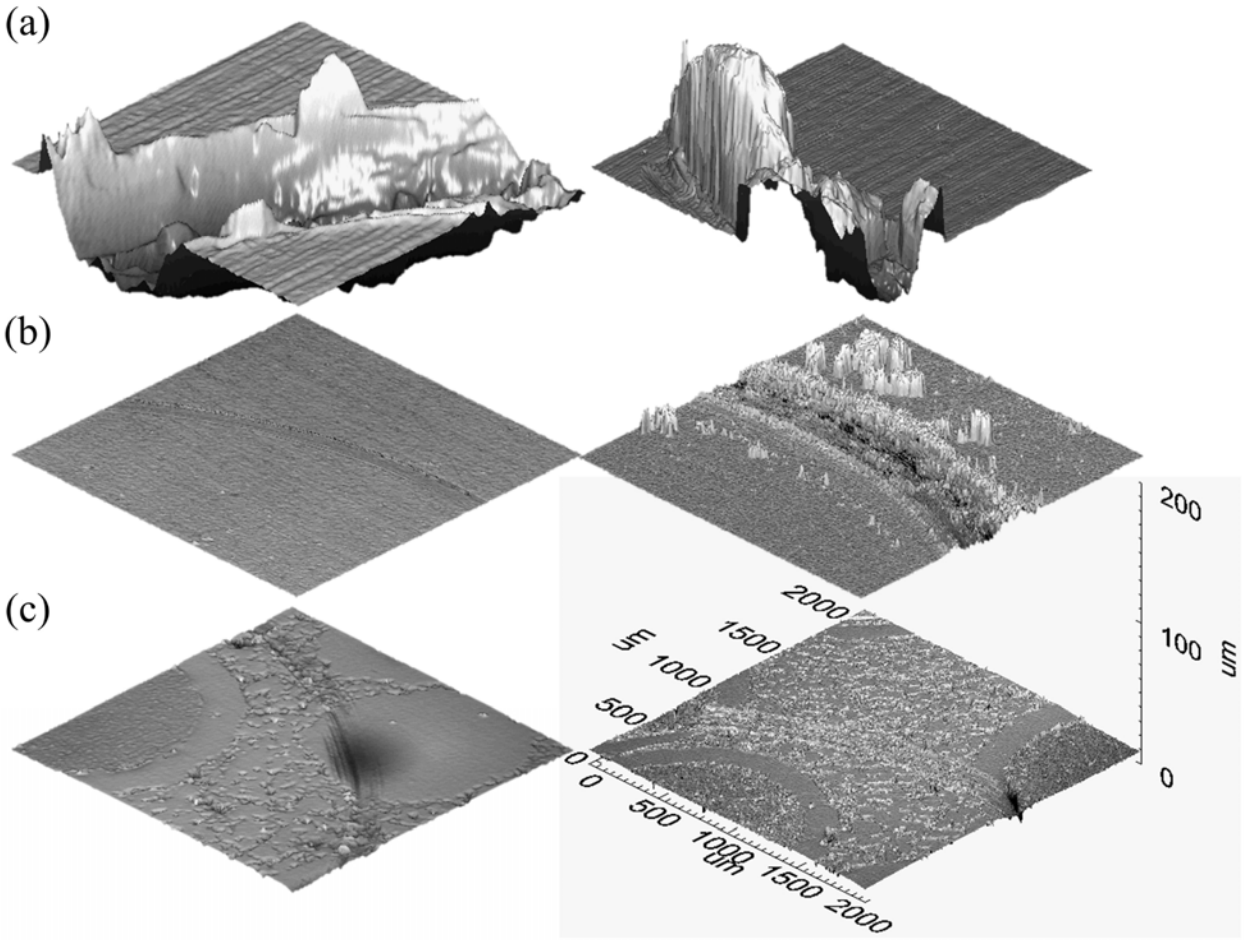

Figure 8. Optical profilometry images taken for bulk aluminum (a), stainless steel (b), and infused SS CMF samples (c) after 50 (left) and 200 (right) revolutions on the PoD tribometer. Each image is displayed at the same scale as indicated in the lower right image.

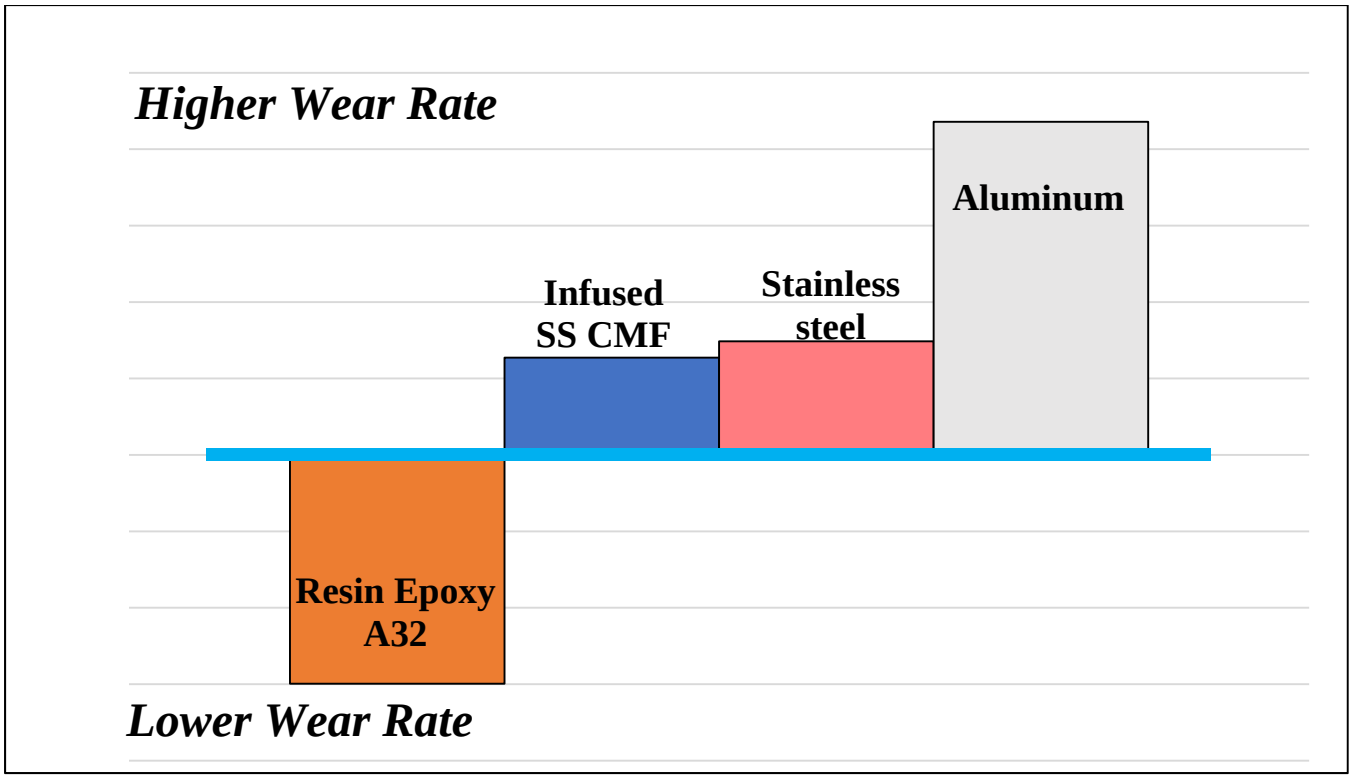

Figure 9. Relative wear rates of each sample measured using the PoD method, when directly compared to each other.

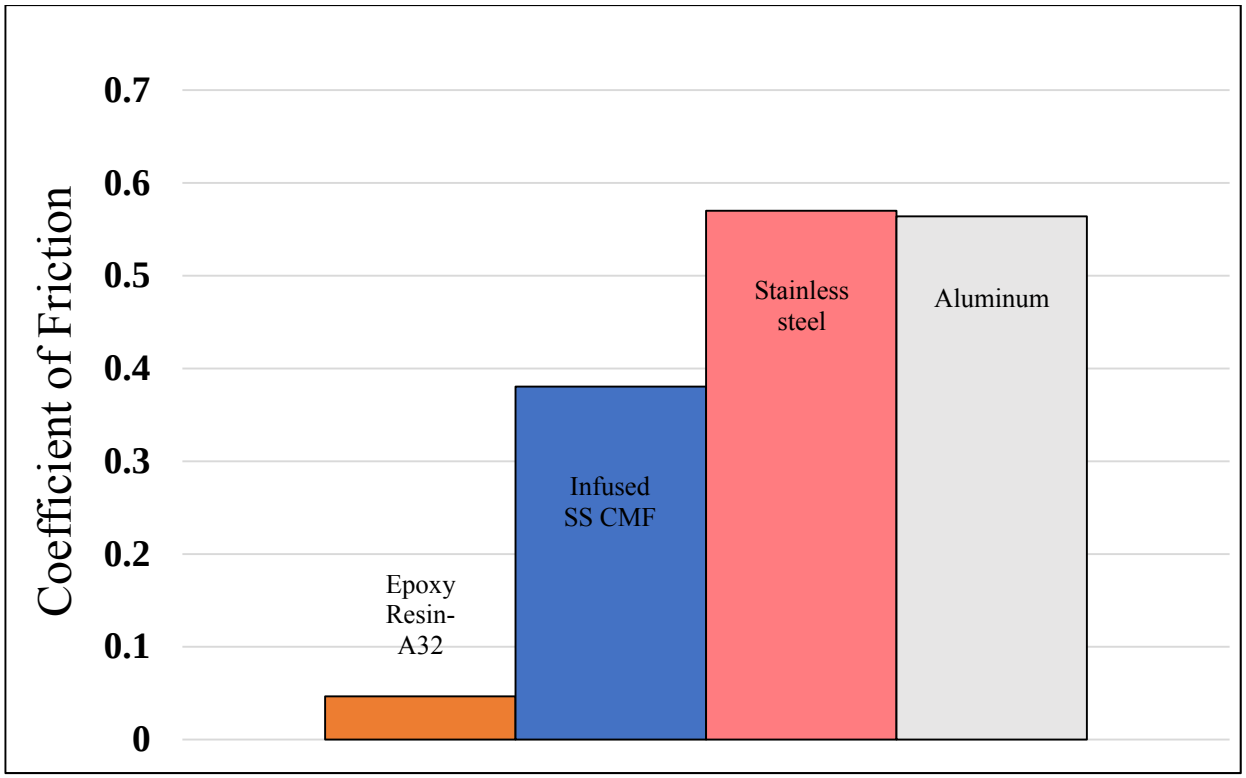

Figure 10. Coefficient of Friction of the initial samples.

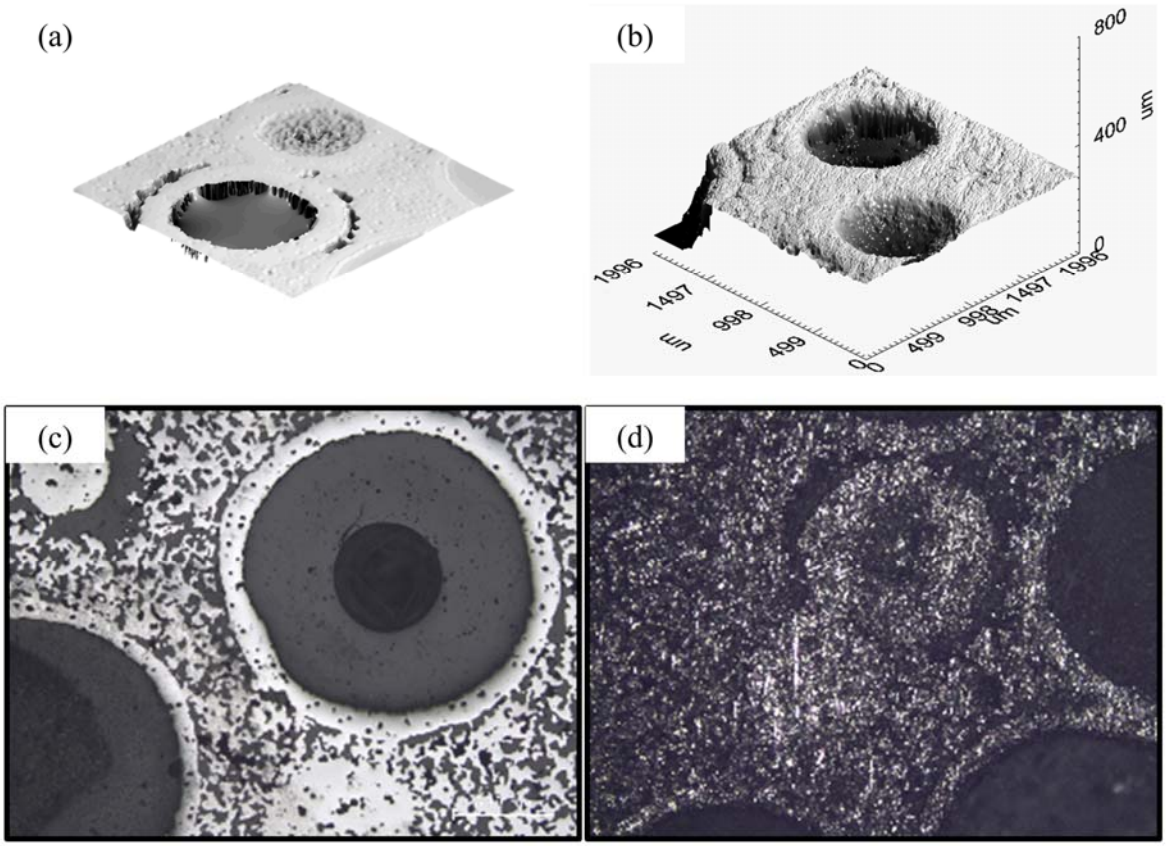

Figure 11. Optical profilometry images of infused SS CMF (a) as polished and (b) after 600 revolutions on the Taber Abraser. Optical microscope images of the (c) polished and (d) abraded surface after 600 revolutions.

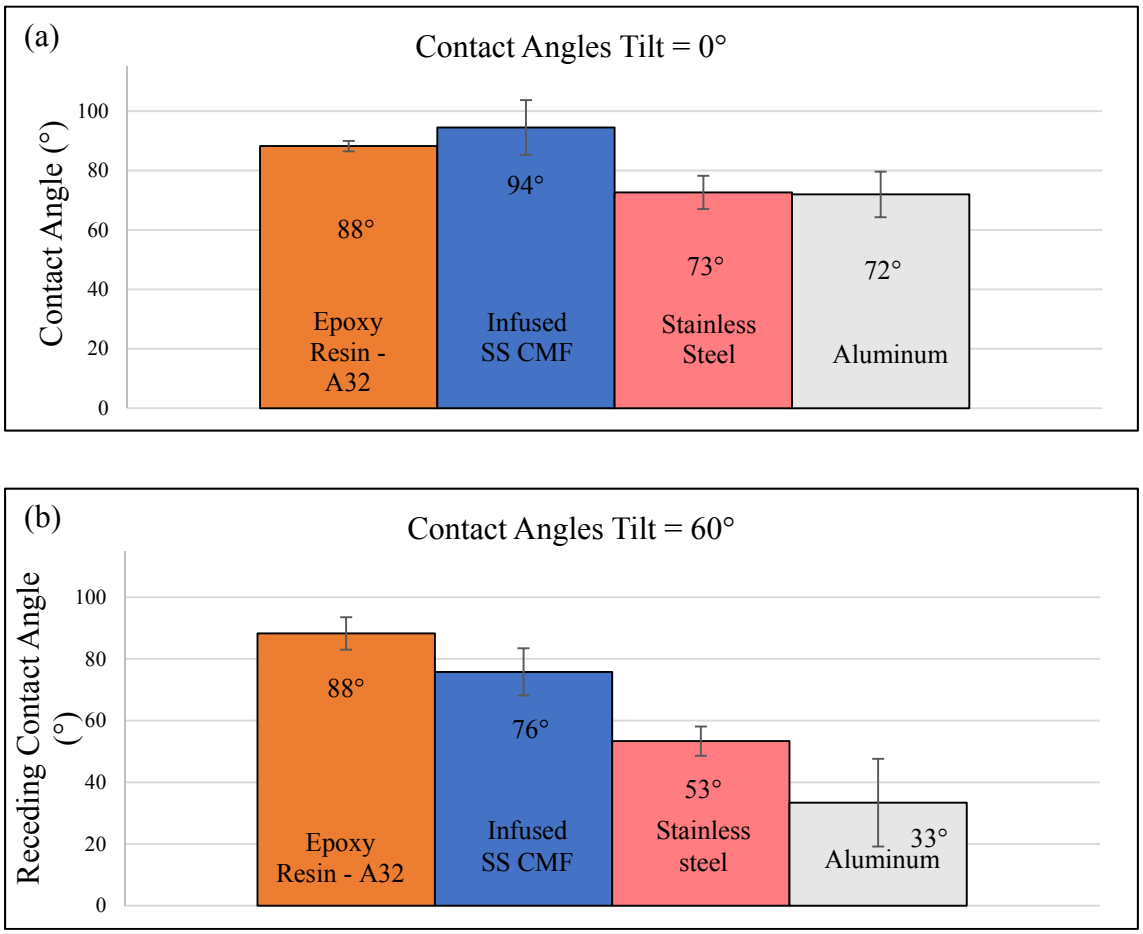

Figure 12. Contact angles measured for each sample at (a) 0º tilt and (b) 60º tilt.

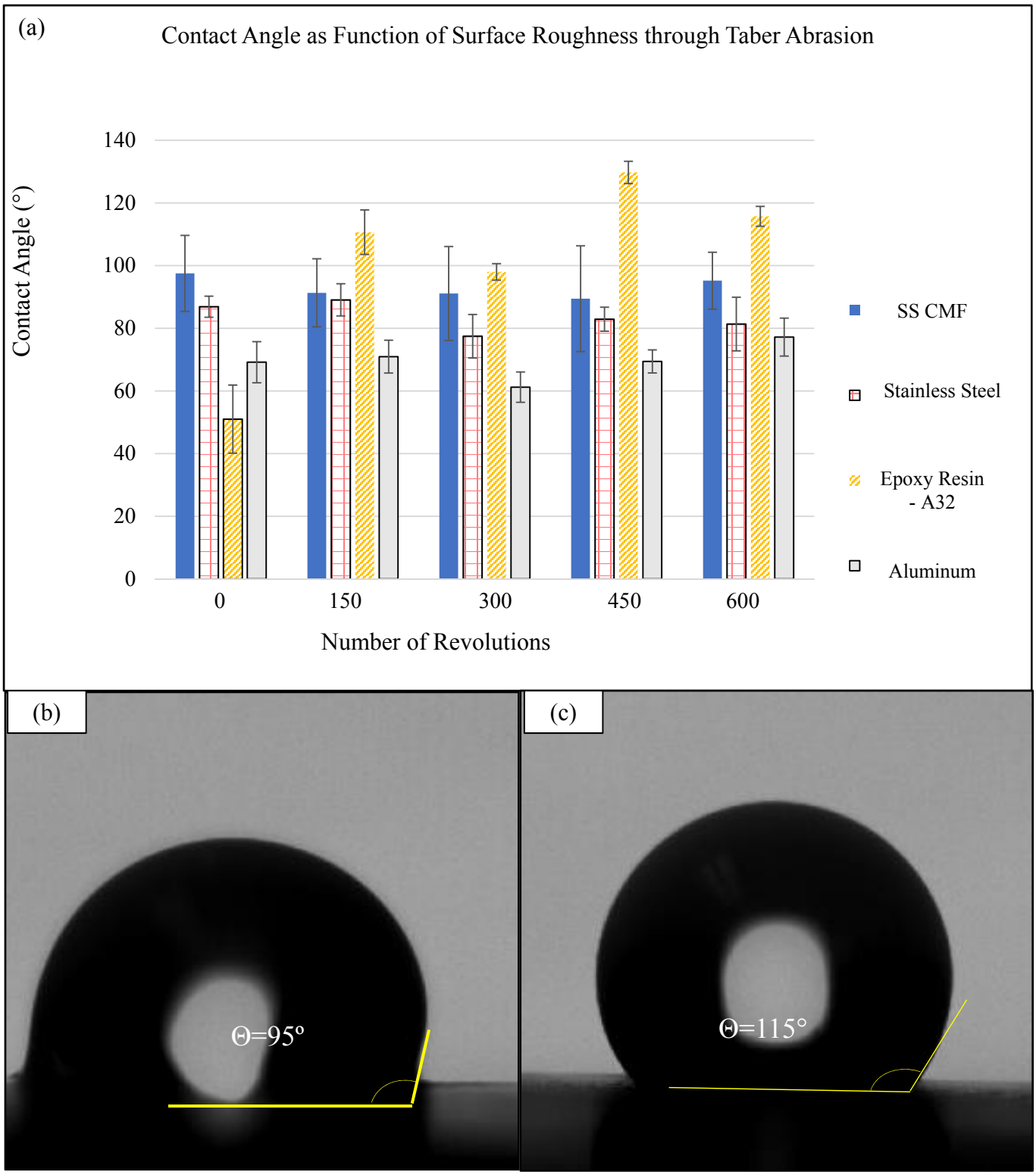

Figure 13. (a) Contact Angle measurements at 0º tilt following set interval of 0, 150, 300, 400, and 600 revolutions in the Taber Abrasion test. (b) and (c) show the contact angle of epoxy infused SS CMF and neat epoxy, respectively.

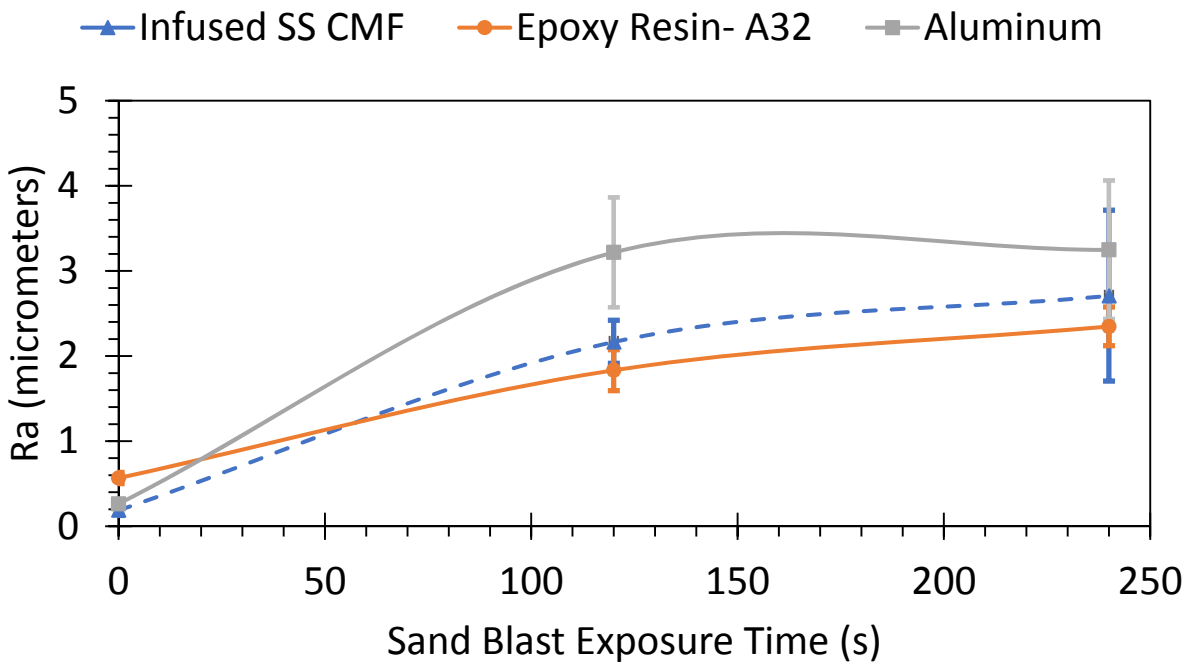

Figure 14: Average surface roughness (R_a) of the infused SS CMF, neat epoxy coupon, and aluminum 2024 samples at multiple intervals of sand blast exposure.

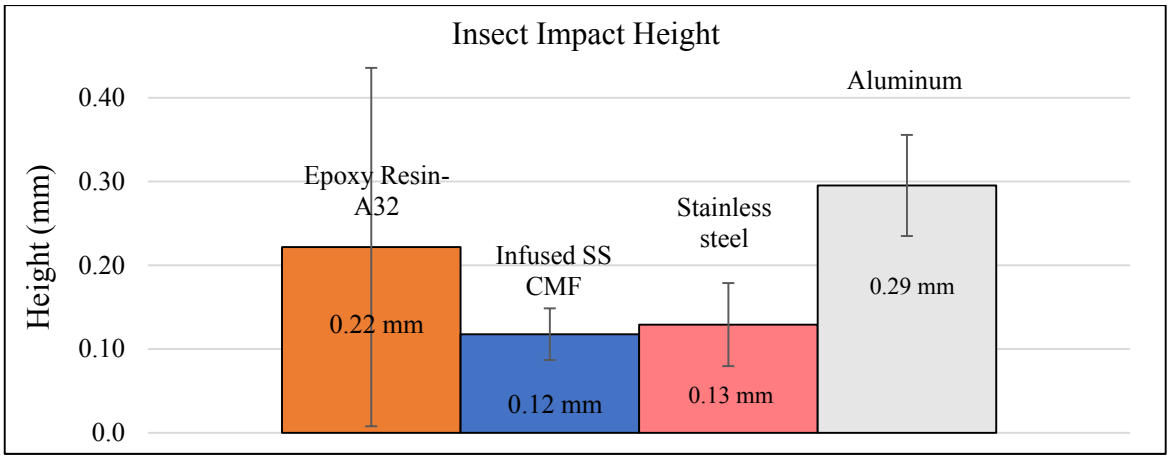

Figure 15. Insect impact adhesion height measured in mm.

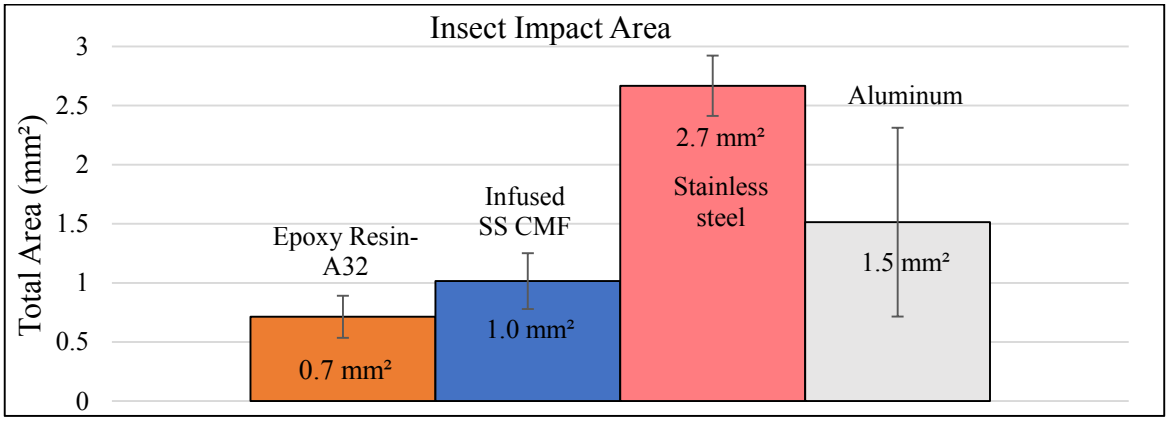

Figure 16. Insect impact area measured in mm^2.

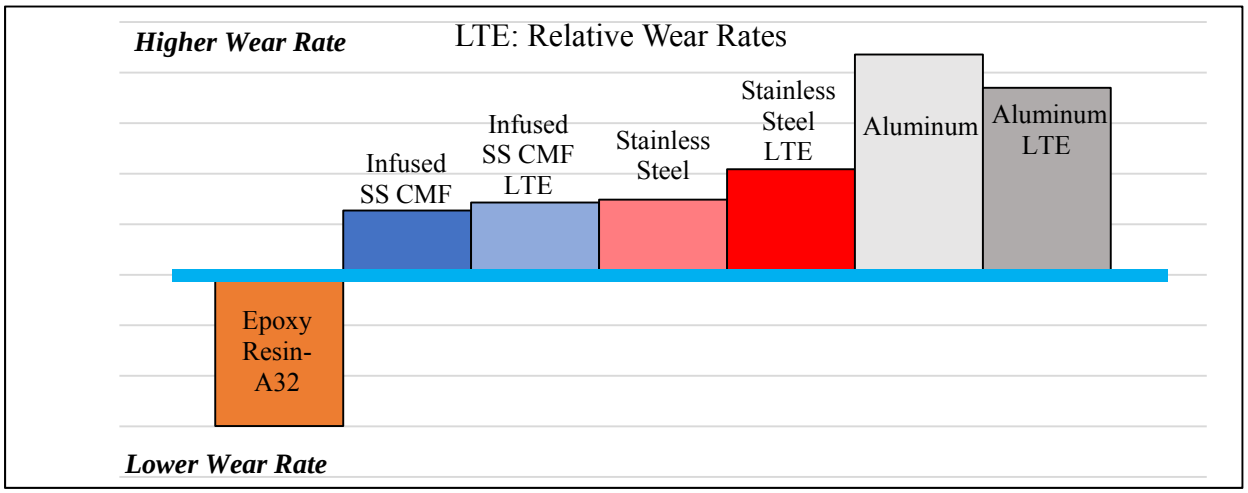

Figure 17. Relative wear rates measured using PoD method of as polished and LTE samples.

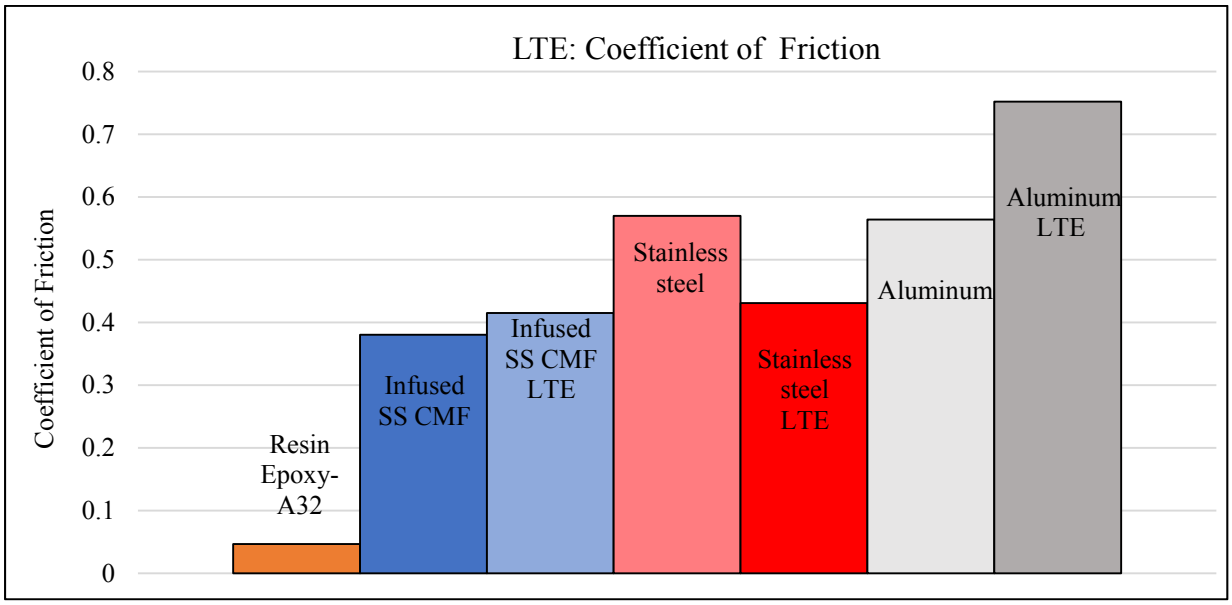

Figure 18. Coefficient of Friction of LTE specimens.

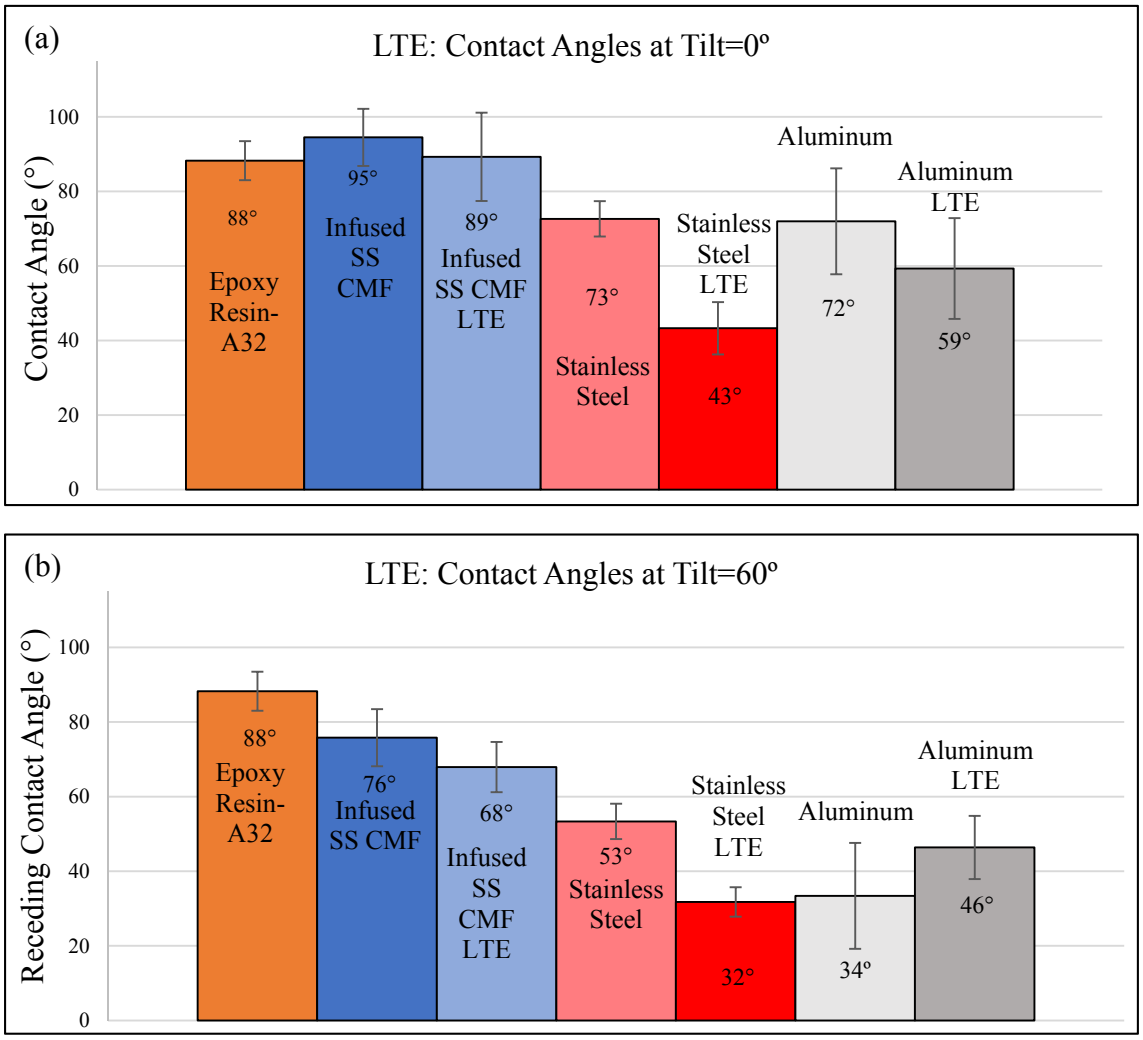

Figure 19. Contact angle at (a) 0º tilt and (b) 60º tilt, on samples that went through the LTE test.

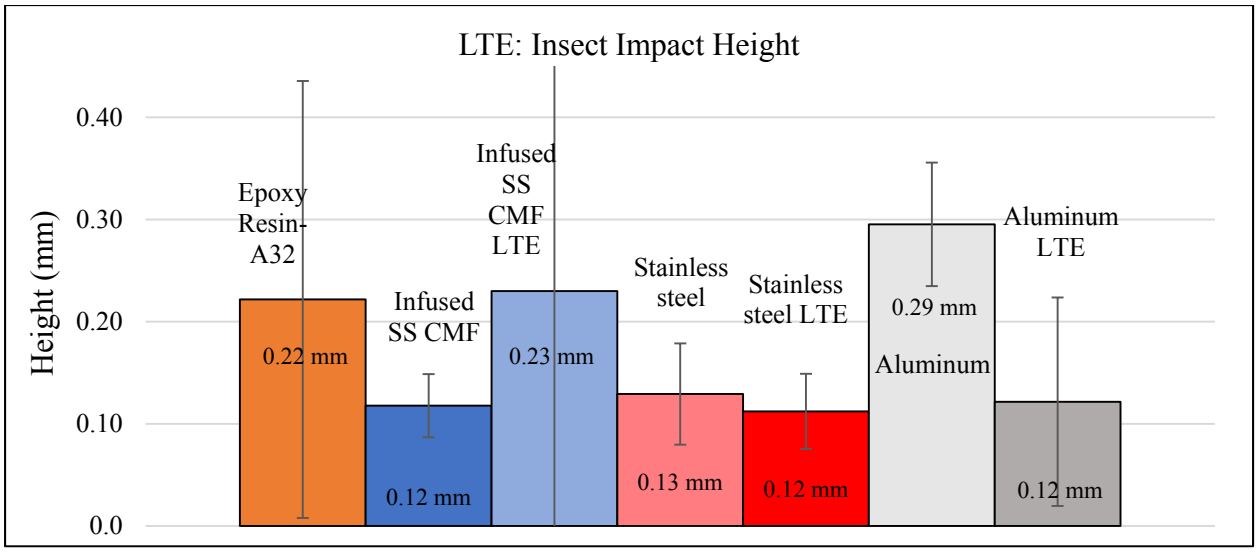

Figure 20. Insect impact adhesion height for LTE samples measured in mm.

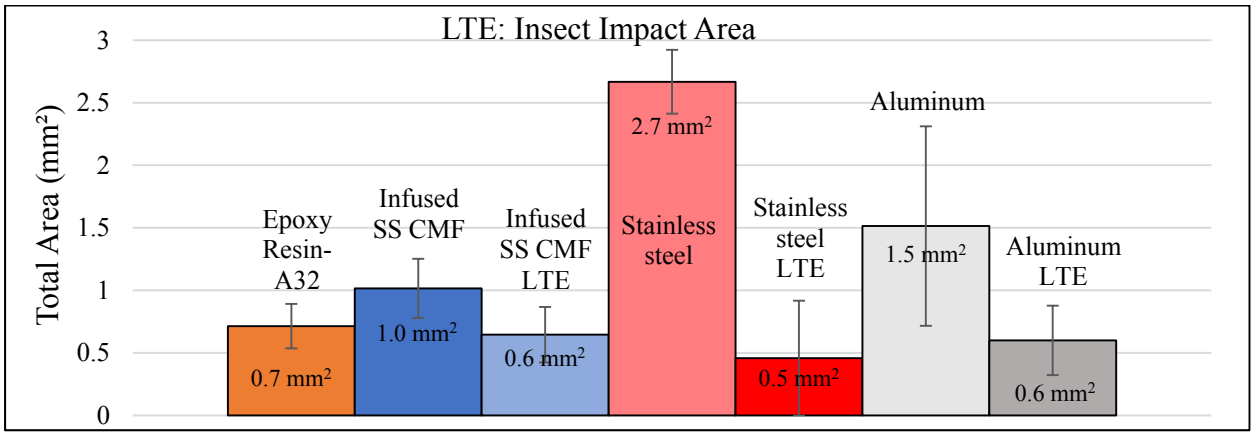

Figure 21. Insect impact adhesion area on samples that went through the LTE test, measured in mm^2.

Table 1. Overview of experiments conducted.

Test		As Polished	Long-Term Erosion	Sample Shape & Sizing (mm)	Surface Finish (μm)
Tribology	Pin on Disk	✓	✓	Flat 50.8 x 50.8	0.22
	Taber Abrasion	✓	-	Cylindrical 36.5 diameter x 13 height	0.18
Contact Angle	0º	✓	✓	20 x 40 x 8	0.22
	60º	✓	✓	20 x 40 x 8	0.22
Surface Erosion Rate		✓	-	50.8 x 76.2	-
Surface Roughness Evolution		✓	-	50.8 x 76.2	-
Insect Adhesion		✓	✓	100 x 50 x 15	0.22

Table 2. Depth of wear following 120 seconds of micro-grit sandblasting.

Sample	Depth (μm)	Wear Rate (μm/s)
Epoxy Resin- A32	325	2.7
Infused SS CMF	104	0.9
Stainless steel	27	0.2